Check for updates

A microfluidics vapor-membrane-valve generated by laser irradiation on carbon nanocoils†

Yuli Liu, [ID] [a] Chengwei Li,[b] Ming Zhao,[c] Jian Shen*[d] and Lujun Pan [ID] *[b]

We have investigated a micro vapor membrane valve (MVMV) for closing the microfluidic channels by laser irradiation on carbon nanocoils (CNCs) attached to the inner wall of the microchannels. The microchannel with MVMVs was found to exhibit a "closed" state without the supply of laser energy, which is explained on the basis of the theory of heat and mass transfer. Multiple MVMVs for sealing the channels can be generated in sequence and exist simultaneously at different irradiation sites, independently. The significant advantages of the MVMV generated by the laser irradiation on CNCs are the elimination of extrinsic energy required to maintain the microfluidic channel "closed" state and the simplification of the structure integrated into the microfluidic channels and fluid control circuitries. The CNC-based MVMV is a powerful tool for the investigations of the functions of microchannel switching and sealing on microfluidic chips in biomedicine, chemical analysis and other fields. The study of MVMVs will have great significance for biochemical and cytological analysis.

Introduction

In recent years, microfluidic chips have been widely used due to their small device size and low energy consumption in various industries such as biology, medicine, manufacturing, and microfluidic technology.[1,2] The controlling of microflow transport is the key technology for microfluidic chips.[3–5] The purpose of controlling microflow transport is actuating reagents and samples throughout different parts of the microfluidic channel. Typically, microvalves are designed to realize regular flow regulation, on/off switching, switch of the fluid, sealing of bio-molecules and so on.[6,7] So far, microfluidic valves have been widely used in drug screening, cell analysis, cell capture, analysis of biological small molecules (such as nucleic acid, protein, etc.) and other fields of life analysis chemistry.[8,9] However, most valves, such as a normally closed valve,[10] shut-off valve,[11] surface tension plug and monolithic elastomer valves,[12] need to be integrated into microfluidic channels. Due to the limit of size, integrating the valves into a microfluidic channel is very complicated.[10]

Currently, microbubbles have received much concern for dynamically commutating or switching fluid transport.[13,14] The rapid swell and collapse of cavitation bubble is used to realize the microfluidic functions, including droplet generation,[15] fluid pumping,[16] cell sorting[17] and high-speed microparticle.[18] The main mechanism of the bubble disruption and actuation is massive pressure exerting on the surrounding liquid and structures (e.g., the inner wall of microfluidic channel) during the bubble cavitation. The advantage of microfluidic valve with microbubbles generated by laser directly induced liquid is no need for complex components or circuits in microstructures, which is meaningful for the manufacture of chip in microfluidic systems, micro-electro-mechanical systems, etc.

However, in order to lower the threshold energy of bubble cavitation, a variety of dyes are usually introduced into a liquid phase, leading to polluting the samples in channels.[19–21] In addition, active oxygen species and free-electrons having a deleterious effect on biomolecule are also created in the liquid medium during rupture processes of bubble cavitation.[22–24]

Carbon nanocoils (CNCs) as a coiled carbon nanomaterials have been confirmed to have excellent near infrared photophysical properties.[25–28] Carbon nanocoils have been used for microbubble generation in our previous work. When the laser beam is focused on a single CNC immersed in deionized water, the energy from the laser beam is absorbed by the CNC because of the unique helix structure and excellent photothermal conversion properties of the CNCs.[29] The thermal energy from the CNC heats the surrounding liquid, which leads to a micro vapor bubble created at the irradiation site. Laser irradiation on the CNC to generate a microbubble, avoiding the employment

[a]Fundamental Education Department, Dalian Neusoft University of Information, Dalian 116023, China. E-mail: liuyuli20052005@163.com; liuyuli@neusoft.edu.cn; Tel: +86 411 82379525

[b]School of Physics, Dalian University of Technology, Dalian 116024, China. E-mail: lpan@dlut.edu.cn; chengweili@dlut.edu.cn; Tel: +86 411 84707863 334

[c]Faculty of Vehicle Engineering and Mechanics, Dalian University of Technology, Dalian 116024, China. E-mail: zhaoming@dlut.edu.cn

[d]Department of Criminal Technology, Liaoning Police College, Dalian 116036, China. E-mail: m13942036212@163.com; Tel: +86 411 86705610

† Electronic supplementary information (ESI) available. See DOI: https://doi.org/10.1039/d3ra01148h

of light absorption dyes and the generation of reactive oxygen species and free-electrons in microfluidic channel.

Additionally, CNCs constructed by a hybrid of amorphous sp^3 and sp^2 graphite grains, not only have the basic characteristics of carbon nanomaterials, but also have the unique catalytic activity, physical and chemical properties, *etc.* It is widely used in many fields, such as optics, catalyst and bio-pharmaceutical, *etc.*[30–32] Sun and coworkers have reported the use of CNC/TiO_2 as photocatalyst for degrading organic contaminants in water under visible light by the redox reactions. Their research results show that CNC/TiO_2 as photocatalyst can degrade more than 50% of organic contaminants in 30 min.[33] Additionally, carbon nanocoils have good chemical stability and excellent biocompatibility, which can avoid to damage biological tissues or cells and to affect the physiological functions of the biomolecule. So CNCs are very suitable for application in the field of biochemistry. Wang and coworkers have reported that CNC-based needle tips are used for the investigations of living cell local mechanical transduction and electrophysiological characteristics.[31] In order to accelerate the development of microfluidic technology in the fields of blood typing, preliminary screening of blood diseases and rapid screening of tumor cells, we use the CNCs with excellent photothermal conversion property and good biocompatibility as a carrier of heating to generate a microvavle for biochemical and cytological analysis.

In this work, we present a new method to control the directional flow of microfluid and realize the switch function for the microfluidic channel through the micro vapor membrane valve (MVMV) evolved from micro vapor bubble, which is realized by the laser irradiation on the carbon nanocoils attached to the inner wall of microfluidic channel. Limited to the channel size, the created vapor bubble evolves into vapor membrane as a valve for clogging the microchannel. This method can maintain multiple independent MVMVs to close microfluidic channels in the desired position of channels with no need for integrating circuits, wiring and microelectrodes on the microfluidic chip.

Materials and methods

The main material of the microfluidic chip used in our experiments is polydimethylsiloxane (PDMS). Microchannels with rectangular cross section in PDMS chip are 20 μm in height, 20 to 100 μm in width. The flowing liquid in all channels were actuated by syringe pump.

The chemical vapor deposition was used to synthesize CNCs with average coil diameter from 300 nm to 600 nm and an average pitch of 200 nm in this experiment (Fig. S1, ESI†).[34] The mixed solution of $Fe_2(SO_4)_3/SnCl_2$ was used as the catalyst precursor for the preparation of CNCs. Fourier transform infrared spectroscopy, X-ray photoelectron spectroscopy and X-ray diffraction patterns of the CNCs are provided in Fig. S2 (ESI†). In our experiment, in order to obtain the CNCs attached to the inner wall of microfluidic channel, the CNCs powder (2 mg) were placed into the deionized water (10 ml) and treated by ultrasonic for 45 min in room temperature to prepare the CNCs
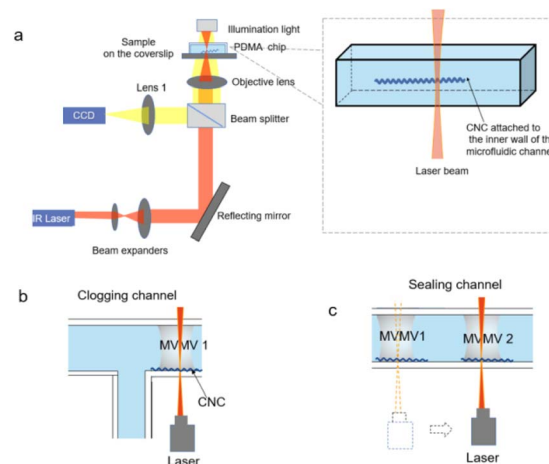

Fig. 1 (a) Experimental set up of laser systems and geometry of the enlarged microchannel with deionized water (blue), CNCs (helix) attached to the inner wall of microfluidic channel. (b) An MVMV for clogging the microchannel. (c) Two MVMVs for stealing the channel.

solution. The CNCs solution was infused into the microfluidic channel by syringe pumps. Then, controlling the deionized water flows into microchannels until no CNCs are suspended in the channel, but only CNCs attached to the inner wall of the channels as shown in Fig. 2a.

The schematic illustration for MVMV generation and applications on microchips is shown in Fig. 1. The laser source is a linearly polarized laser diode with a wavelength of 1064 nm and laser spot diameter of 4 μm, approximately. The laser beam is focused through a 60X objective lens system (1.25 numerical aperture) on CNCs attached to the inner wall of the microfluidic channels in PDMS chip.

The dynamic process of the MVMV generation by laser irradiation was captured through a microscope coupled with a 60X objective, a charge coupled device camera system, computer software and a mobile phone with photographic function.

Results and discussion

Fig. 2a shows the CNCs that attached to the inner wall of microchannel due to liquid pressure between liquid and PDMS, van der Waals attraction, and excellent flexibility of the CNCs. In addition, CH_3 functional group in PDMS is easily adsorbed to wrinkles of the CNCs, which is helpful for CNCs attaching to the walls of channel.[33] The TEM image of a single CNC (in the inset of Fig. 2a, high magnification TEM pictures in Fig. S3, ESI†) shows that CNC has a unique spiral structure which benefits the heat accumulation on the pitch of CNCs immersed into deionized water.[29] The Raman spectrum of the channel with CNCs (in Fig. 2b) further proves that the CNCs are attached to the inner wall of the channel.

Fig. 3a shows a hemispheric microbubble is rapidly created in the microchannel by laser irradiation (power of 0.74 mW) on the CNCs attached to the inner wall of microfluidic channel. Fig. 3a and b show the hemispheric microbubble grows over time under continuous laser irradiation. Limited to the size of the channel
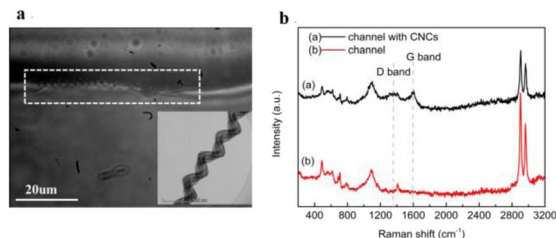
Fig. 2 (a) Optical microscope image of the CNCs attached to the inner wall of the microfluidic channel filled with deionized water and transmission electron microscope of a single CNC in left bottom inset. (b) The Raman shift of the channel with CNCs from the dashed line area in (a).
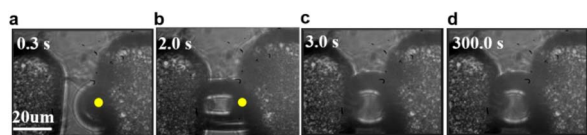

Fig. 3 Optical images of the microchannel with a width of 20 μm clogged by the MVMV evolved from the vapor bubble induced by focused laser irradiation. (a) A hemispheric microbubble immediately created at the irradiation site by laser irradiation for 0.3 s. (b) An MVMV developed from the hemispheric microbubble for clogging the microchannel by laser irradiation for 2 s. (c and d) The MVMV maintained to its initial shape for 300 s without supplying energy from laser irradiation. The yellow dots indicate the irradiation site of the focused laser beam. The focused laser power is 0.74 mW.

(width of 20 μm, height of 20 μm), the vapor bubble evolves into a vapor membrane as an MVMV for closing the microfluidic channel at 2 s after the laser irradiation, as shown in Fig. 3b. With the increasing of irradiation time, the MVMV is elongated along the longitudinal direction of the channel as shown in Fig. 3c. In fact, the heat energy converted from laser beam will be transmitted to the surrounding liquid along the CNC lengthways direction due to the excellent thermal conductivity of CNCs. This suggests that the lengthways size of the MVMV can be adjusted by controlling the laser irradiation time.

To obtain a stabilized and fixed size MVMV, the laser beam is removed from the CNCs after the MVMV formed. An interesting finding is that the MVMV will not shrink and disappear for 300 s after removing the laser beam from the CNCs, as shown in Fig. 3d. It means the channel can remain "closed" state for a long time without supplying energy.

This phenomenon is different from our previous work that spherical vapor bubbles in deionized water, *i.e.* bubbles unconfined by the channel boundaries, begin to shrink obviously when the laser irradiation is shut off.[29] It proves that PDMS channel benefits to prevent dissipation of thermal energy from the bubble to the surrounding liquid and the lifetime of an MVMV is not laser irradiation dependent. The above results mean that the laser as power source can be separated from the MVMV.

To confirm the function of the MVMV, the power of laser is adjusted to 0.95 mW for the larger size channels. Fig. 4a and b show that a wider microfluidic channel (width of 100 μm) is clogged by the MVMV evolved from the microbubble. Similarly,
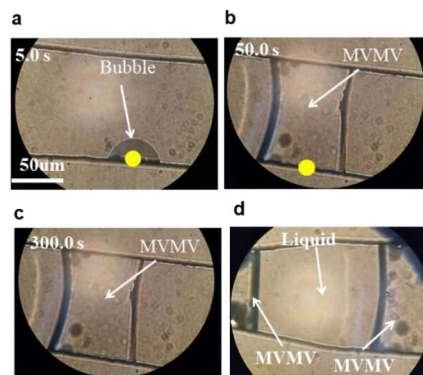

Fig. 4 Microscope images of the MVMVs generated in a wider channel (width of 100 μm). (a) A microbubble is created by 5 s after laser irradiation. (b) A microbubble evolves into an MVMV to close the wider channel by laser irradiation for 50 s. (c) The MVMV without shrinking for 300 s after removing the laser beam from CNCs. (d) Two independent MVMVs generated in sequence to build a sealed channel. The yellow dots indicate the irradiation site of the focused laser beam. The power of laser beam is 0.95 mW.

this MVMV still exists without shrinking for 300 s after removing the laser beam from the CNC, as shown in Fig. 4c. Then, the laser beam with the same laser power of 0.95 mW was focused on another site at the inner wall of channel with CNCs. Another MVMV appears at the new irradiation site and both MVMVs are independent of each other in a shared channel, as shown in Fig. 4d. This result demonstrates multiple independent MVMVs can be formed in sequence by adjusting the irradiation site, which means a sealed channel can be constructed in microfluidic channel.

All these results imply that the MVMV functions, including the plug, switch, seal, *etc.*, can be maintained in the microchannel for a long time with no need for extrinsic energy source after MVMV formed, which is very useful in microfluidic chip, nanoelectronic devices and micro-electromechanical systems.

Comparing with our previous work,[29] similar theories are used to analyze bubble generation, the bubble growth and the MVMV evolution in the microfluidic channel.

At the initial stage of bubble generation, the dynamics theories of bubble nucleation suggest that activation energy is required to squeeze the surrounding liquid in the site of the heating surface.[35] The minimum of activation energy required can be obtained with the help of external conditions such as grooves or slits at the heating surface. Analogously, the concave spaces of spiral CNC act as the grooves or slits of heating surface, which benefit the formation of bubbles. When the laser beam is precisely focused on the CNCs, the photon energy of the beam will be absorbed by CNCs and converted into heat energy used to vaporize the liquid at the area of laser irradiation. A microbubble is created on the CNC irradiated by laser beam.

After the generation of bubble, the growth of the bubble and the evolution of the MVMV in the microfluidic channel can be analyzed by the mass and heat transfer theory which is similar to that used in our previous work.[29] The specific enthalpy increment per unit time in vapor bubble is attributable to the

heat transfer and laser irradiation, which could be explained by the following formula:

$$m_g c_{p,g} \frac{dT_g}{dt} = -hA(T_g - T_d) + Q, \tag{1}$$

where m_g is the vapor mass inside the bubble, $c_{p,g}$ is the specific heat capacity at constant pressure inside the bubble. T_g and T_d denote the temperature inside bubble and liquid surrounding bubble, respectively. h is the surface heat transfer coefficient and A is the bubble surface area while Q denotes the laser power. The specific enthalpy increment of liquid is attributable to the heat transfer from bubble to liquid and the heat absorption of liquid evaporation. Thus the specific enthalpy increment in liquid per unit time can be described as below,

$$m_d c_{p,d} \frac{dT_d}{dt} = hA(T_g - T_d) + q_{m,d} \cdot r, \tag{2}$$

where m_d is the liquid mass, $c_{p,d}$ denotes the specific heat capacity of the liquid at constant pressure, $q_{m,d}$ denotes the evaporation rate of the liquid, and r is the latent heat for vaporizing liquid. The mass flux transported into the bubble can be described as

$$q_{m,v} = M_d h_D A(c_{v0} - c_{v\infty}), \tag{3}$$

where M_d, h_D, c_{v0} and $c_{v\infty}$ are the molar mass of the liquid, surface mass transfer coefficient, the vapor concentration on the bubble surface, and the vapor concentration inside the bubble, respectively. In the case of ideal gas, we get

$$c_{v0} - c_{v\infty} = \frac{n_{v0}}{V_{v0}} - \frac{n_{v\infty}}{V_{v\infty}} = \frac{1}{R}\left(\frac{p_{v0}}{T_d} - \frac{p_{v\infty}}{T_g}\right), \tag{4}$$

where p_{v0} is the bubble surface vapor pressure, $p_{v\infty}$ is the vapor pressure inside the bubble and R is the molar vapor constant. Also in eqn (4), $q_{m,v}$ is given by mass conservation law as

$$-q_{m,d} = q_{m,v} = \frac{dm_g}{dt} = \frac{d}{dt}\left(\frac{\pi d^3 \rho_g}{6}\right), \tag{5}$$

where d is the bubble diameter and ρ_g is the vapor density inside the bubble.

In eqn (1)–(4), the bubble surface area A is crucial to the development of bubble. The smaller A is, the slower the heat transfer is. The temperature rise rate inside the bubble is faster than the outside of the bubble. Higher temperature difference between the internal and external bubble causes a rapid evaporation of the liquid around the bubble and a mass increase of the gas inside the bubble. Finally, the volume of the bubble increases gradually with a further increasing of the temperature. Overall, after the stage of bubble generation, the bubble will expand with the increasing of laser irradiation time.

The experiments show that the bubble expands with the increasing of laser irradiation time. When the developing bubble touches the inner walls of microchannel, a vapor membrane with surface area A is formed. Moreover, the vapor membrane keeps elongating along the longitudinal direction of microfluidic channel under laser irradiation. It means that the vapor membrane does not reach its maximum size when the

surface area of the vapor membrane is A. Thus, the mass and heat transfer between the vapor membrane and the liquid surrounding the membrane does not reach a balance. The bubble temperature T_g does not reach the maximum which implies that $m_g c_{p,g} \frac{dT_g}{dt}$ in eqn (1) is not equal to zero while vapor membrane does not reach its maximum size. Since the liquid surrounding vapor membrane cannot be regarded as infinite (the four surfaces of the vapor membrane are enclosed by PDMS channels with good thermal insulation property), the temperature T_d of the liquid surrounding the vapor membrane with surface area A will rise and the temperature difference $(T_g - T_d)$ will decrease gradually under laser irradiation. Therefore, when the focused laser is shut off, i.e., Q becomes zero, the absolute value of heat transfer term $|-hA(T_g - T_d)|$ in eqn (1) is relatively small since both the area of heat transfer and the temperature difference between the liquid and the vapor are relatively small in the membrane case, which means the heat inside the vapor membrane will not be transmitted to the liquid quickly, and the temperature and volume of the vapor membrane will not be changed very quickly over time. Thus, the vapor membrane is able to exist stably in microfluidics channel for a long time after removing the laser beam from the CNCs.

In addition, we also found that the vapor bubble shrinks gradually then thoroughly disappears when the laser beam is removed from the CNCs, as shown in Fig. 5. It can also be explained by the similar theories in eqn (1). For vapor bubble in microchannels, the external environment (the liquid surrounding bubble in the channel) can be approximately infinite with respect to the microbubble size. So when the heat inside the bubble is transferred to the outside of the bubble, the liquid temperature T_d can be regard as a constant, approximately. The temperature difference between vapor bubble and liquid $(T_g - T_d)$ is higher than that between vapor membrane and liquid. Therefore, when the focused laser is shut off, i.e., Q becomes zero, the absolute value of heat transfer term $|-hA(T_g - T_d)|$ is relatively large since both the area of heat transfer and the temperature difference between the liquid and the vapor are relatively large in the bubble case. In comparison with the vapor membrane, the temperature and volume of the vapor bubble will be significantly reduced. This suggests that the microchannel is crucial for the lifetime of stable vapor membrane.

Considering the effect of flow rate on the expansion of hemispherical bubble, we investigate the relationship between the diameter of the hemispherical bubble and the laser irradiation time within 12 s at various volumetric flow rates. In this study, we ignore the change of the bubble shape and assume that the bubble shape is developed approximately from
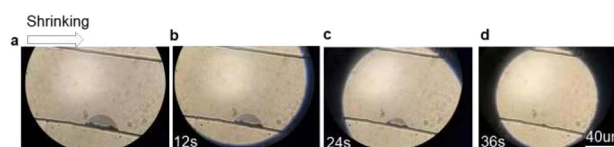

Fig. 5 Dynamics of the bubble contraction after removing the laser beam from the CNCs.
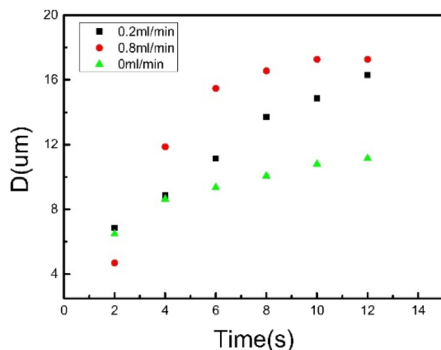
Fig. 6 Expansion curves of vapor bubble with time under different flow rates.

Fig. 7 Microscope images of an MVMV that can perform "close–reopen" cycles. (a) The channel at "closed" state after an MVMV generated by laser irradiation for 1 min (The power of laser beam is 1.08 mW). The yellow dots indicate the irradiation site of the focused laser beam. (b) The channel at "reopened" state after the flow rate of 0.8 ml min^{-1} with 1 min.

hemispherical to spherical during the bubble expansion. Fig. 6 shows that the expansion rate of hemispherical bubble increases significantly with an increasing flow rate. It is clear that hemispheric bubbles are easier to expand in fluid with a higher flow rate. A hypothesis could, thus, be that the increased expansion rate of bubble with an increasing flow rate is owing to the fluid flows accelerating the heat dissipation inside bubble.[36,37]

The fluid flow rate in microchannel does not prevent the generation of microbubbles, but help the formation of the MVMV for clogging the channels. The higher the fluid flow rate is, the shorter the formation time of the MVMV. It is also found that, at the early stage of nucleation, the higher the flow rate is, the smaller the radius of the nuclear hemispherical bubble. Actually, a research on the problem shows that at the early stage of the bubble generation, the area to volume ratio of the heat transfer from vapor to liquid is relatively large considering the small radius of bubble. Higher flow rate corresponds to larger convective coefficient of heat transfer, *i.e.*, larger h in $-hA(T_g - T_d)$. Therefore, the heat flux from vapor to liquid is increased for higher flow rate, leading to smaller radius of vapor bubble. However, for later stage, the flow path (channel) is partially blocked by a growing bubble, leading to a narrowed flow path for fluid flow. When the fluid flow through the narrowed channel, the fluid flow will be accelerated.[38] A higher flow rate in the narrow channel will lower the pressure at the narrowed channel, which is the outside of the bubble. Bernoulli equation still works for the fluid flow in our microfluid channels, ignoring the viscous force (although strictly speaking, Bernoulli equation works for inviscid flow).[38] Thus, the lowered pressure helps the bubble to grow, which is similar to Bernoulli effect. Larger inflow induces larger pressure drop, which benefits the growth of the bubble.

Moreover, the development speed of microbubble is rapidly fast at the initial stage and then gradually slow down as shown in Fig. 6, which can also be explained by eqn (1)–(4). The bubble surface area A is still crucial to the development of bubble. When the surface area A is small, the heat transfer from the bubble to liquid is slow and the temperature difference between the internal and external bubble is relatively large. Therefore, the liquid evaporates quickly. By contrast, when the surface area
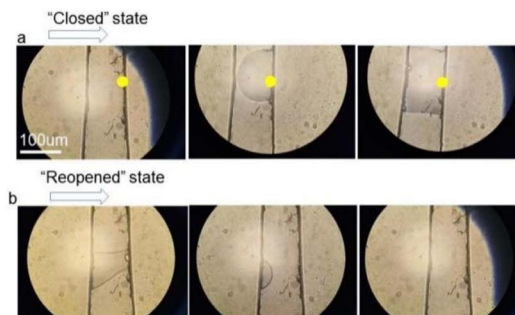
A is large, the heat transfer is fast and the temperature difference is relatively small. Therefore, the liquid evaporates slowly.

To recover the channel "open" state, the flow rate of liquid is considered to help the MVMV shrink. Fig. 7b shows the closed channel was reopened by increasing the flow rate to 0.8 ml min^{-1} with 1 min. The "closed" and "reopened" states of channel are realized by the MVMV as shown in Fig. 7. The flowing liquid accelerates the speed of heat dispersion, which is beneficial to transfer the heat from the membrane to the liquid and to lower the internal pressure of the membrane. Therefore, there is a pressure difference between the inside and the outside membrane. When the external force acting on the surface of membrane is greater than the surface tension on the gas–liquid phase interface, the pressure of the internal and the external membrane cannot be balanced by the surface tension and the pressure component acting on the membrane causes the shape depression and the size reduction of the membrane.[39] As the heat dissipation is ongoing, the shaped depression of membrane is strengthened and the volume of membrane is reduced gradually (Fig. S4, ESI†). In the meantime, the contact area between the membrane and the inner walls of channel will be reduced and the angle between gas–solid line and gas–liquid line will become smaller. When the angle between the gas–solid line and the gas–liquid line is smaller than the wetting angle of membrane, *i.e.*, the separation condition for membrane from the inner walls of channel, the membrane will be torn off the inner walls and deformed to the bubble which will shrink gradually then thoroughly disappear. The channel is opened again, as shown in Fig. 7b.

Conclusions

We have demonstrated a method to generate a vapor membrane as an MVMV in microfluidic channels by laser irradiation. This experiment is realized by utilizing laser irradiation on the CNCs attached on the inner wall of the microchannels to generate a vapor bubble evolving into a vapor membrane for closing the microchannels. The results show that a laser beam with 0.74 mW power can induce an MVMV for the microchannel with

a width of 20 μm and a height of 20 μm. And the vapor membrane can be maintained for a long time with no need for the supplying of laser irradiation. Moreover, the flow rate of the fluid can accelerate the formation of the MVMV due to the heat dissipation effect. By changing the laser irradiation site, multiple MVMVs can be generated in sequence and exists simultaneously at different sites, independently. The main advantage of the MVMV generated by the laser irradiation on CNCs is the elimination of extrinsic energy required to maintain microfluidic channel "closed" state. This method is significant to simplify the structure integrated into the microfluidic channels and fluid control circuitries.

Combined with laser irradiation, CNCs-based MVMVs are investigated for typical microfluidic channel of the traditional microfluidic chip for the first time. The CNCs-based MVMV can precisely control the opening or closing and switching of the flow channels by laser irradiation. The MVMV is easy used in many types of microfluidic channel since the size of MVMV matched to channels can be controlled by laser power. The CNC-based MVMV is a powerful tool for the investigations of the functions of microchannels switching and sealing on the microfluidic chip in biomedicine, chemical analysis and other fields. We envision the future use of the CNCs-based MVMV for blood, sweat, urine, and a variety of chemical reagents condition. Microfluidic chip with CNCs-based MVMV will be an effective tool for blood typing, preliminary screening of blood diseases, rapid screening of tumor cells and rapid nucleic acid detection performed on the microfluidic chips.

Author contributions

Yuli Liu and Chengwei Li: characterization, photoacoustic imaging, experiment, theoretical analysis and manuscript writing; Ming Zhao: theoretical analysis; Jian Shen and Lujun Pan: design and supervise the project, manuscript revision, and corresponding authors.

Conflicts of interest

There are no conflicts to declare.

Acknowledgements

Notes and references

1 G. M. Whitesides, The origins and the future of microfluidics, *Nature*, 2006, **442**, 368–373.

2 X. Shengqing, N. Zhihong, S. Minseok, L. Patrick, K. Eugenia, A. S. Howard, G. Piotr, B. W. Douglas, G. Irina and M. W. George, Generation of monodisperse particles by using microfluidics: control over size, shape, and composition, *Angew. Chem., Int. Ed.*, 2005, **44**, 653–827.

3 T. Todd, J. M. Sebastian and R. Q. Stephen, Microfluidic Large-Scale Integration, *Science*, 2002, **298**, 580–584.

4 H. Bo, W. Hongkai, B. Devaki, *et al.*, Counting Low-Copy Number Proteins in a Single Cell, *Science*, 2007, **315**, 81–84.

5 M. Masahiro, S. Jun, A. Dai and H. Shinji, Noncontact manipulation of microflow by photothermal control of viscous force, *Int. J. Heat Fluid Flow*, 2010, **31**, 1005–1011.

6 F. G. Tseng, C. J. Kim and C. M. Ho, Symposium on Applications of Micro-fabrication to Fluid, *Mechanics*, 1998, **66**, 89–95.

7 S. S. Yong, *et al.*, A passive microfluidic valve fabricated from a hydrogel filled with carbon nanotubes, *Carbon*, 2012, **50**, 1417–1421.

8 K. Sungbong, Z. Yi, W. Sangmin, B. J. Amay, S. Yurina, X. Yeguang, K. Jahyun, H. W. Sean, M. A. Jennifer, P. Jeong Min, R. R. Tyler, C. E. Kaitlyn, L. Kyu-Tae, C. Jungil, P. L. Rhonda, G. C. Claude, S. J. Adam, C. YuYu, X. Shuai, K. Jeonghyun, K. Ahyeon, H. Jeongsook, H. Yonggang, K. Seungwook and R. A. John, Super-Absorbent Polymer Valves and Colorimetric Chemistries for Time-Sequenced Discrete Sampling and Chloride Analysis of Sweat *via* Skin-Mounted Soft Microfluidics, *Small*, 2018, **14**, 1703334, DOI: **10.1002/smll.201703334**.

9 Z. Yingxue, C. Yao, H. Jielong, L. Yangchengyi, P. Jinfeng, C. Shangda, S. Kui, O. Xiaoping, C. Huanyu and W. Xiufeng, Skin-interfaced microfluidic devices with one-opening chambers and hydrophobic valves for sweat collection and analysis, *Lab Chip*, 2020, **2**, 2635–2645.

10 M. Ritika, R. S. Benjamin, V. D. Amit, *et al.*, Design considerations for elastomeric normally closed microfluidic valves, *Sens. Actuators, B*, 2011, **160**, 1216–1223.

11 R. D. Lovchik, N. Tonna, F. Bianco, *et al.*, A microfluidic device for depositing and addressing two cell populations with intercellular population communication capability, *Biomed. Microdevices*, 2010, **12**, 275–282.

12 M. Sifeng, Z. Jie, L. Haifeng and L. Jinming, Strategy for Signaling Molecule Detection by Using an Integrated Microfluidic Device Coupled with Mass Spectrometry to Study Cell-to-Cell Communication, *Anal. Chem.*, 2013, **85**, 868–876.

13 K. D. Aditya, A. D. Jayashree, V. M. Amit, *et al.*, Dynamics of Photothermally Created Vaporous, Gaseous, and Mixed Microbubbles, *J. Phys. Chem. C*, 2011, **115**, 6611–6617.

14 J. Amanda, A. S. Theresia, T. S. Klas, *et al.*, Chemical delivery array with millisecond neurotransmitter release, *Sci. Adv.*, 2016, **2**, e1601340.

15 P. S. Yong, W. T. Hsiang, C. Yue, *et al.*, High-speed droplet generation on demand driven by pulse laser-induced cavitation, *Lab Chip*, 2011, **11**, 1010–1012.

16 R. Dijkink and C. D. Ohl, Laser-induced cavitation based micropump, *Lab Chip*, 2008, **8**, 1676–1681.

17 W. T. Hsiang, C. Yue, P. S. Yong, *et al.*, Pulsed laser triggered high speed microfluidic fluorescence activated cell sorter, *Lab Chip*, 2012, **12**, 1378–1383.

18 W. T. Hsiang, G. Lanyu, C. Yue, *et al.*, Pulsed laser triggered high speed microfluidic switch, *Appl. Phys. Lett.*, 2008, **93**, 144102.

19 P. A. Quinto-Su, X. H. Huang, S. R. Gonzalez-Avila, *et al.*, Manipulation and Microrheology of Carbon Nanotubes with Laser-Induced Cavitation Bubbles, *Phys. Rev. Lett.*, 2010, **104**, 014501.

20 K. T. Chung and C. E. Cerniglia, Mutagenicity of azo dye: Structure-activity relationships, *Mutat. Res.*, 1992, **277**, 201–220.

21 D. Rawat, R. S. Sharma, S. Karmakar, *et al.*, Ecotoxic potential of a presumably nontoxic azo dye, *Ecotoxicol. Environ. Saf.*, 2018, **148**, 528–537.

22 A. Vogel, J. Noack, G. Huttman and G. Paltauf, Mechanisms of femtosecond laser nanosurgery of cells and tissues, *Appl. Phys. B: Lasers Opt.*, 2005, **81**, 1015–1047.

23 A. Singh, R. Kukreti, L. Saso and S. Kukreti, Oxidative Stress: A Key Modulator in Neurodegenerative Diseases, *Molecules*, 2019, **24**, 1583.

24 M. Isaguliants, S. Olga, A. V. Ivanov, *et al.*, Oxidative stress induced by HIV-1 reverse transcriptase modulates the enzyme's performance in gene immunization, *Hum. Vaccines Immunother.*, 2013, **9**, 2111–2119.

25 W. Peng, P. Lujun, L. Cheng Wei and Z. Jia, Highly Efficient Near-Infrared Photothermal Conversion of a Single Carbon Nanocoil Indicated by Cell Ejection, *J. Phys. Chem. C*, 2018, **122**, 27696–27701.

26 M. Barrejón, L. M. Arellano, H. B. Gobeze, *et al.*, N-Doped graphene/C60 covalent hybrid as a new material for energy harvesting, applications, *Chem. Sci.*, 2018, **9**, 8221–8227.

27 M. He, P. Lujun, Z. Qin, *et al.*, Electrically driven light emission from a single suspended carbon nanocoil, *Carbon*, 2012, **50**, 5537–5542.

28 M. He, P. Lujun, Z. Qin and P. Wei, Near-Infrared Response of a Single Carbon Nanocoil, *Nanoscale*, 2013, **5**, 1153–1158.

29 S. Yanming, P. Lujun, L. Yuli and S. Tao, Micro-Bubble Generated by Laser Irradiation on an Individual Carbon Nanocoil, *Appl. Surf. Sci.*, 2015, **345**, 428–432.

30 R. B. Rakhi, D. Cha, W. Chen and H. N. Alshareef, Electrochemical Energy Storage Devices Using Electrodes Incorporating Carbon Nanocoils and Metal Oxides Nanoparticles, *J. Phys. Chem. C*, 2011, **115**, 14392–14399, DOI: **10.1021/jp202519e**.

31 W. Peng, G. Chunyang, P. Lujun and L. Bo, A carbon nanocoil-based flexible tip for a live cell study of mechanotransduction and electro-physiological characteristics, *J. Mater. Chem. B*, 2020, **8**, 1405–1410.

32 W. Peng, P. Lujun, L. Chengwei and J. Zheng, Optically Actuated Carbon Nanocoils, *Nano*, 2018, **13**, 1793–2920.

33 L. Xin, S. Yanming, Z. Zhenyu, *et al.*, Visible light-driven multi-motion modes CNC/TiO$_2$ nanomotors for highly efficient degradation of emerging contaminants, *Carbon*, 2019, **155**, 195–203.

34 Z. Yongpeng, W. Jianzhen, H. Hui, *et al.*, Growth of Carbon Nanocoils by Porous α-Fe$_2$O$_3$/SnO$_2$ Catalyst and Its Buckypaper for High Efficient Adsorption, *Nano-Micro Lett.*, 2020, **12**, 1–17.

35 B. Sundén, *Introduction to heat transfer*, Boston, 2012.

36 P. A. Quinto-Su, M. Suzuki and C. D. Ohl, Fast temperature measurement following single laser-induced cavitation inside a microfluidic gap, *Sci. Rep.*, 2014, **4**, 5445–5450.

37 Y. Yanan, Y. Yafei, L. Yuhang, L. Min and S. Jizhou, Thermal Analysis on Active Heat Dissipation Design with Embedded Flow Channels for Flexible Electronic Devices, *Micromachines*, 2021, **12**, 1165, DOI: **10.3390/mi12101165**.

38 E. G. Sinaiski, *Hydromechanics: Theory and Fundamentals*, German Chemical Society, Singapore, 2011.

39 M. Sussman and P. Smereka, Axisymmetric free boundary problems, *J. Fluid Mech.*, 1997, **341**(341), 269–294.